Semiquantitative Analysis of the Biodistribution of the Combined ^{18}F-NaF and ^{18}F-FDG Administration for PET/CT Imaging

Ryogo Minamimoto[1,2], Camila Mosci[1], Mehran Jamali[1,2], Amir Barkhodari[1], Frezghi Habte[2], Tatianie Jackson[1], Erik Mittra[1], Sanjiv Sam Gambhir[1,2], and Andrei Iagaru[1]

[1]*Division of Nuclear Medicine and Molecular Imaging, Department of Radiology, Stanford University, Stanford, California; and* [2]*Department of Radiology, Molecular Imaging Program at Stanford, Stanford University, Stanford, California*

In this study, we evaluated the biodistribution of the ^{18}F$^-$/^{18}F-FDG administration, compared with separate ^{18}F-NaF and ^{18}F-FDG administrations. We also estimated the interaction of ^{18}F-NaF and ^{18}F-FDG in the ^{18}F$^-$/^{18}F-FDG administration by semiquantitative analysis. **Methods:** We retrospectively analyzed the data of 49 patients (39 men, 10 women; mean age ± SD, 59.3 ± 15.2 y) who underwent separate ^{18}F-FDG PET/CT and ^{18}F-NaF PET/CT scans as well as ^{18}F$^-$/^{18}F-FDG PET/CT sequentially. The most common primary diagnosis was prostate cancer (n = 28), followed by sarcoma (n = 9) and breast cancer (n = 6). The mean standardized uptake values (SUVs) were recorded for 18 organs in all patients, and maximum SUV and mean SUV were recorded for all the identified malignant lesions. We also estimated the ^{18}F$^-$/^{18}F-FDG uptake as the sum of ^{18}F-FDG uptake and adjusted ^{18}F-NaF uptake based on the ratio of ^{18}F-NaF injected dose in ^{18}F$^-$/^{18}F-FDG PET/CT. Lastly, we compared the results to explore the interaction of ^{18}F-FDG and ^{18}F-NaF uptake in the ^{18}F$^-$/^{18}F-FDG scan. **Results:** The ^{18}F$^-$/^{18}F-FDG uptake in the cerebral cortex, cerebellum, parotid grand, myocardium, and bowel mostly reflected the ^{18}F-FDG uptake, whereas the uptake in the other analyzed structures was influenced by both the ^{18}F-FDG and the ^{18}F-NaF uptake. The ^{18}F$^-$/^{18}F-FDG uptake in extraskeletal lesions showed no significant difference when compared with the uptake from the separate ^{18}F-FDG scan. The ^{18}F$^-$/^{18}F-FDG uptake in skeletal lesions reflected mostly the ^{18}F-NaF uptake. The tumor-to-background ratio of ^{18}F$^-$/^{18}F-FDG in extraskeletal lesions showed no significant difference when compared with that from ^{18}F-FDG alone (P = 0.73). For skeletal lesions, the tumor-to-background ratio of ^{18}F$^-$/^{18}F-FDG was lower than that from ^{18}F-NaF alone ($P < 0.001$); however, this difference did not result in missed skeletal lesions on the ^{18}F$^-$/^{18}F-FDG scan. **Conclusion:** The understanding of the biodistribution of radiopharmaceuticals and the lesion uptake of the ^{18}F$^-$/^{18}F-FDG scan as well as the variations compared with the uptake on the separate ^{18}F-FDG PET/CT and ^{18}F-NaF PET/CT are valuable for more in-depth evaluation of the combined scanning technique.

Key Words: ^{18}F-NaF; ^{18}F-FDG; PET/CT; SUV

J Nucl Med 2015; 56:688–694
DOI: 10.2967/jnumed.115.153767

Received Jan. 6, 2015; revision accepted Mar. 12, 2015.
For correspondence or reprints contact: Andrei Iagaru, Division of Nuclear Medicine and Molecular Imaging, Department of Radiology, Stanford University Medical Center, Stanford, 300 Pasteur Dr., Stanford, CA 94305-5281.
E-mail: aiagaru@stanford.edu
Published online Apr. 3, 2015.

PET/CT with ^{18}F-FDG is a valuable tool for staging and monitoring response to therapy in various cancers (*1*). However, due to variable rates of glucose metabolism, not all cancer lesions are identified reliably (*1*). ^{18}F-sodium fluoride (^{18}F-NaF) is currently used for bone scintigraphy with integrated PET/CT scanners (*2–7*). The combined administration of ^{18}F-NaF and ^{18}F-FDG (^{18}F$^-$/^{18}F-FDG) in a single PET/CT scan for cancer detection has been advocated for detecting both extraskeletal and skeletal lesions in a single visit (*8,9*), and the early prospective multicenter trial indicated promising results (*10*).

In this study, we performed a semiquantitative analysis to evaluate the biodistribution of the ^{18}F$^-$/^{18}F-FDG administration, compared with the separate ^{18}F-NaF and ^{18}F-FDG administrations. We also investigated the relationship between uptake and several factors such as the dosage and the time from injection to imaging.

MATERIALS AND METHODS

Patients

The local Institutional Review Board and Cancer Center Scientific Review Committee approved the study. Written informed consent was obtained from all patients. Between September 2007 and December 2013, 79 consecutive participants with pathologically proven malignancy underwent ^{18}F$^-$/^{18}F-FDG PET/CT and separate ^{18}F-FDG PET/CT and ^{18}F-NaF PET/CT. From these, we included only those with time from tracer injection to imaging within 30 min between ^{18}F$^-$/^{18}F-FDG PET/CT and ^{18}F-FDG PET/CT as well as between ^{18}F$^-$/^{18}F-FDG PET/CT and ^{18}F-NaF PET/CT. Forty-nine patients (men, 39; women, 10; age range, 19–84 y; mean age, 59.3 ± 15.2 y) fit the inclusion criteria for this analysis and were previously reported for feasibility of the scanning method (*8*). The primary diagnosis included prostate cancer (n = 28), sarcoma (n = 9), breast cancer (n = 6), colon cancer (n = 1), lung carcinoma (n = 1), bladder cancer (n = 1), gastrointestinal stromal tumor (n = 1), renal cell cancer (n = 1), and urothelial cancer (n = 1).

PET/CT Protocol

The patients were scanned on a Discovery LS, 600, or 690 scanner (GE Healthcare). There were only small (<10%) differences in standardized uptake value (SUV) measurements between scanners based on data from phantom studies. All 3 scans were acquired on the same scanner for all patients. Patients were asked to fast for 6 h before injection of ^{18}F-FDG and ^{18}F$^-$/^{18}F-FDG. No patient preparation was required for the ^{18}F-NaF PET/CT scans. For the ^{18}F$^-$/^{18}F-FDG PET/CT scans, the 2 radiotracers were delivered from the local

TABLE 1
Details of 3 Types of PET Scans

Parameter	$^{18}F^{-}/^{18}F$-FDG	^{18}F-FDG	^{18}F-NaF
Injection dose (MBq)	$^{18}F^{-}/^{18}F$-FDG: 625.1 ± 85.8	478.2 ± 85.0	248.7 ± 84.0
	^{18}F-FDG: 426.9 ± 82.7		
	^{18}F-NaF: 199.7 ± 35.5		
Time from injection to imaging (min)	76.6 ± 13.0	75.5 ± 13.8	75.2 ± 17.7
The difference in time of starting PET/CT with $^{18}F^{-}/^{18}F$-FDG PET/CT (min)	—	1.1 ± 13.0	1.3 ± 15.0
Time interval of PET/CT with $^{18}F^{-}/^{18}F$-FDG PET/CT (d)	—	4.1 ± 4.7	4.1 ± 4.4

cyclotron facilities in separate syringes and administered sequentially, without delay. For all PET/CT scans, total body (vertex to toes) PET/CT images were obtained in 2-dimensional mode for Discovery LS and 3-dimensional mode for Discovery 600 and 690, with the patients' arms at their sides. The PET images were reconstructed with a standard iterative algorithm (ordered-subset expectation maximization, 2 iterative steps and 28 subsets for Discovery LS, 2 iterative steps and 32 subsets for Discovery 600, and 2 iterative steps and 24 subsets for Discovery 690).

Image Analysis

Images were the reformatted into axial, coronal, and sagittal views and reviewed by 2 board-certified nuclear medicine physicians using MIMvista software (MIMvista Corp.) to determine the uptake in normal tissues and lesions. A board-certified nuclear medicine physician with 8 y experience in PET/CT diagnosis placed regions of interest (ROIs) in the frontal lobe cortex, cerebellum, parotid grand, lung, myocardium, left atrium cavity (blood pool), liver, spleen, pancreas, kidney, bowel (cecum), trapezius muscle, gluteus maximus muscle, gluteal fat, third cervical vertebrae, ninth thoracic vertebrae, third lumbar vertebrae, and sacrum. Circular ROIs (diameter, 10–30 mm) were then drawn on transaxial PET images and carefully positioned over the central portion of each normal structure depicted on the PET/CT image. For the myocardium, a circular ROI with a 10-mm diameter was placed on the lateral wall of the left atrium, with the edge adjusted to be outside the edge placed for blood-pool ROI. For the blood pool, a circular ROI with a 20-mm diameter was placed

TABLE 2
Radiopharmaceutical Uptake (SUV_{mean}) for Studied Organs, Based on Time from Injection to Imaging

	Time from injection to imaging (min)								
	$^{18}F^{-}/^{18}F$-FDG			^{18}F-FDG			^{18}F-NaF		
Organ	52–60 (n = 6)	60–90 (n = 32)	90–104 (n = 11)	43–60 (n = 8)	60–90 (n = 35)	90–111 (n = 6)	39–60 (n = 10)	60–90 (n = 29)	90–117 (n = 10)
Brain cortex (frontal lobe)	10.4 ± 2.4	9.7 ± 2.4	10.4 ± 2.5	10.0 ± 2.0	10.2 ± 2.5	11.2 ± 2.5	0.2 ± 0.1	0.3 ± 0.1	0.3 ± 0.1
Cerebellum	8.5 ± 1.8	8.2 ± 1.9	8.6 ± 2.0	8.2 ± 1.9	8.7 ± 1.9	9.2 ± 1.2	0.2 ± 0.1	0.2 ± 0.1	0.2 ± 0.1
Parotid grand	2.1 ± 0.9	1.9 ± 0.7	1.5 ± 0.4	1.6 ± 0.9	2.1 ± 1.1	1.4 ± 0.6	0.6 ± 0.2	0.5 ± 0.1	0.4 ± 0.1
Lung	0.7 ± 0.2	0.6 ± 0.2	0.7 ± 0.2	0.4 ± 0.2	0.5 ± 0.1	0.6 ± 0.1	0.3 ± 0.1	0.4 ± 0.2	0.4 ± 0.1
Myocardium	4.3 ± 2.4	4.8 ± 4.1	4.0 ± 4.0	3.7 ± 2.6	4.3 ± 3.9	7.7 ± 7.1	0.6 ± 0.3	0.7 ± 0.2	0.6 ± 0.2
Left atrium (background)	2.7 ± 0.7	2.3 ± 0.6	2.2 ± 0.6	1.8 ± 0.5	1.8 ± 0.4	1.9 ± 0.3	1.1 ± 0.4	1.2 ± 0.4	0.9 ± 0.3
Liver	2.6 ± 0.6	2.3 ± 0.5	2.5 ± 0.6	2.0 ± 0.5	2.2 ± 0.4	2.2 ± 0.3	0.4 ± 0.1	0.5 ± 0.2	0.4 ± 0.1
Spleen	2.2 ± 0.4	1.8 ± 0.6	2.3 ± 1.1	1.8 ± 0.6	1.7 ± 0.5	1.9 ± 0.3	0.6 ± 0.2	0.7 ± 0.2	0.5 ± 0.2
Pancreas	1.9 ± 0.3	1.7 ± 0.5	1.5 ± 0.6	1.4 ± 0.3	1.5 ± 0.4	1.2 ± 0.4	0.6 ± 0.2	0.6 ± 0.2	0.6 ± 0.2
Kidney	3.1 ± 0.8	2.7 ± 0.8	2.9 ± 1.1	2.4 ± 0.6	2.4 ± 0.6	2.0 ± 0.5	1.2 ± 0.5	1.7 ± 0.8	1.3 ± 0.5
Cecum	1.6 ± 0.4	1.7 ± 1.4	1.8 ± 1.8	0.9 ± 0.3	1.8 ± 2.0	1.0 ± 0.5	0.6 ± 0.2	0.7 ± 0.4	0.5 ± 0.1
Trapezius muscle	1.0 ± 0.3	1.0 ± 0.3	1.0 ± 0.3	0.6 ± 0.1	0.6 ± 0.1	0.7 ± 0.1	0.7 ± 0.2	0.8 ± 0.2	0.8 ± 0.2
Gluteus maximus muscle	1.0 ± 0.4	0.9 ± 0.3	1.1 ± 0.4	0.6 ± 0.2	0.7 ± 0.2	0.6 ± 0.1	0.7 ± 0.3	0.8 ± 0.2	0.7 ± 0.2
Fat tissue	0.3 ± 0.1	0.4 ± 0.2	0.4 ± 0.2	0.3 ± 0.1	0.3 ± 0.2	0.2 ± 0.1	0.2 ± 0.1	0.3 ± 0.1	0.2 ± 0.1
Cervical vertebrae	4.9 ± 2.6	4.5 ± 1.5	5.0 ± 2.7	1.3 ± 0.6	1.3 ± 0.3	1.7 ± 0.5	7.2 ± 3.1	6.9 ± 2.2	7.3 ± 2.5
Thoracic vertebrae	6.0 ± 2.9	5.0 ± 1.6	5.3 ± 2.5	1.8 ± 0.7	1.7 ± 0.6	1.6 ± 0.5	7.0 ± 2.5	7.6 ± 2.1	7.2 ± 2.0
Lumbar vertebrae	5.6 ± 2.4	4.8 ± 1.9	4.9 ± 3.0	1.5 ± 0.4	1.7 ± 0.6	1.5 ± 0.7	6.7 ± 1.6	7.1 ± 2.4	6.3 ± 2.4
Sacrum	4.9 ± 2.5	3.8 ± 1.5	4.2 ± 3.0	1.1 ± 0.3	1.2 ± 0.5	1.6 ± 0.1	5.8 ± 2.2	5.7 ± 2.3	5.3 ± 2.8

TABLE 3
SUV_{mean} Measurements from PET Scans

Organ	SUV_{mean}			Comparison of $^{18}F^{-}/^{18}F$-FDG and ^{18}F-FDG	
	$^{18}F^{-}/^{18}F$-FDG	^{18}F-FDG	^{18}F-NaF	*P*	Correlation (r)
Brain cortex (frontal lobe)	10.0 ± 2.4	10.3 ± 2.4	0.2 ± 0.1	0.32	0.62
Cerebellum	8.4 ± 1.9	8.7 ± 1.8	0.2 ± 0.1	0.51	0.49
Parotid grand	1.8 ± 0.7	1.9 ± 1.0	0.5 ± 0.2	0.77	0.75
Lung	0.6 ± 0.2	0.5 ± 0.1	0.4 ± 0.1	<0.001	0.76
Myocardium	4.5 ± 3.8	4.6 ± 4.3	0.7 ± 0.2	0.94	0.69
Left atrium (background)	2.3 ± 0.6	1.8 ± 0.4	1.1 ± 0.4	<0.001	0.71
Liver	2.4 ± 0.5	2.2 ± 0.4	0.5 ± 0.2	<0.007	0.60
Spleen	2.0 ± 0.7	1.7 ± 0.5	0.6 ± 0.2	<0.001	0.60
Pancreas	1.7 ± 0.5	1.5 ± 0.4	0.6 ± 0.2	0.001	0.46
Kidney	2.8 ± 0.8	2.4 ± 0.6	1.5 ± 0.7	0.003	0.28
Cecum	1.7 ± 1.4	1.6 ± 1.7	0.7 ± 0.3	0.30	0.75
Trapezius muscle	1.0 ± 0.3	0.6 ± 0.1	0.8 ± 0.2	<0.001	0.50
Gluteus maximus muscle	1.0 ± 0.3	0.7 ± 0.2	0.7 ± 0.2	<0.001	0.68
Fat tissue	0.4 ± 0.2	0.3 ± 0.2	0.2 ± 0.1	<0.001	0.85
Cervical vertebrae	4.7 ± 1.9	1.4 ± 0.4	7.0 ± 2.4	<0.001	0.51
Thoracic vertebrae	5.2 ± 2.0	1.7 ± 0.6	7.4 ± 2.1	<0.001	0.65
Lumbar vertebrae	4.9 ± 2.2	1.6 ± 0.6	6.8 ± 2.2	<0.001	0.71
Sacrum	4.0 ± 2.0	1.3 ± 0.5	5.7 ± 2.3	<0.001	0.66

TABLE 4
SUV_{mean} of $^{18}F^{-}/^{18}F$-FDG in Studied Organ and Differences from Estimated $^{18}F^{-}/^{18}F$-FDG Values

Organ	$^{18}F^{-}/^{18}F$-FDG	Estimated $^{18}F^{-}/^{18}F$-FDG	Comparison of $^{18}F^{-}/^{18}F$-FDG and estimated $^{18}F^{-}/^{18}F$-FDG	
			P	Correlation (r)
Brain cortex (frontal lobe)	10.0 ± 2.4	10.4 ± 2.4	0.17	0.62
Cerebellum	8.4 ± 1.9	8.8 ± 1.8	0.26	0.49
Parotid grand	1.8 ± 0.7	2.2 ± 1.1	<0.003	0.77
Lung	0.6 ± 0.2	0.7 ± 0.2	0.24	0.85
Myocardium	4.5 ± 3.8	5.0 ± 4.3	0.28	0.69
Left atrium (background)	2.3 ± 0.6	2.4 ± 0.6	0.16	0.80
Liver	2.4 ± 0.5	2.4 ± 0.5	0.24	0.64
Spleen	2.0 ± 0.7	2.0 ± 0.5	0.58	0.61
Pancreas	1.7 ± 0.5	1.8 ± 0.5	0.26	0.54
Kidney	2.8 ± 0.8	3.1 ± 0.8	<0.02	0.44
Cecum	1.7 ± 1.4	1.9 ± 1.9	0.58	0.76
Trapezius muscle	1.0 ± 0.3	1.0 ± 0.2	0.39	0.73
Gluteus maximus muscle	1.0 ± 0.3	1.0 ± 0.3	0.52	0.75
Fat tissue	0.4 ± 0.2	0.4 ± 0.2	0.66	0.87
Cervical vertebrae	4.7 ± 1.9	4.8 ± 1.7	0.19	0.77
Thoracic vertebrae	5.2 ± 2.0	5.3 ± 1.8	0.31	0.85
Lumbar vertebrae	4.9 ± 2.2	5.0 ± 1.9	0.47	0.85
Sacrum	4.0 ± 2.0	3.9 ± 1.6	0.94	0.80

centrally within the left atrium at the level of its widest diameter. An ROI with a diameter of 30 mm was placed on the right liver lobe, but it was changed to the left lobe in 2 cases with intensely ^{18}F-FDG–avid metastases in the right hepatic lobe. If metastases were present at the measurement site, ROIs were placed in the opposite area if the structure was symmetric. For metastases seen in the third cervical vertebrae, ninth thoracic vertebrae, and third lumbar vertebrae, ROIs were placed in the adjacent vertebra.

For SUV measurements of malignant lesions, radiologic reports of the separate ^{18}F-FDG PET/CT, ^{18}F-NaF PET/CT, ^{99m}Tc-methylene diphosphonate bone scan, and contrast-enhanced CT as well as clinical follow-up were used to confirm the diagnosis. The CT portion of PET/CT was used for determining the characterization of bone lesions as osteoblastic or osteolytic (including mixed type). The PETedge tool of the MIMvista software was used for SUV measurements in malignant lesions. ROIs for organs were first drawn on ^{18}F$^-$/^{18}F-FDG PET/CT scans with the reference to anatomic structure confirmed by the CT portion of the PET/CT image, and after that the exact same size and shape ROI was put on the ^{18}F-FDG PET/CT and ^{18}F-NaF PET/CT scans. The measurements for SUV in lesions were performed up to 6 lesions per scan in decreasing order of maximum SUV (SUV_{max}).

Data Analysis

For the calculation of SUV, imputed injection dose for ^{18}F$^-$/^{18}F-FDG PET/CT was set as just the dose of ^{18}F-FDG used in the ^{18}F$^-$/^{18}F-FDG PET/CT scan. First, we compared the ^{18}F$^-$/^{18}F-FDG uptake with the ^{18}F-FDG uptake from ^{18}F-FDG PET/CT images, to estimate the influence of ^{18}F-NaF on various organs. If there was no significant difference in the SUV between ^{18}F$^-$/^{18}F-FDG uptake and ^{18}F-FDG uptake, we estimated the region to be mainly the result of the ^{18}F-FDG uptake. In contrast, if the significant differences in the SUV measurement between ^{18}F$^-$/^{18}F-FDG uptake and ^{18}F-FDG uptake were confirmed, we estimated the region as being influenced by both ^{18}F-FDG and ^{18}F-NaF uptake. Next we adjusted the SUV (mean SUV [SUV_{mean}] or SUV_{max}) of ^{18}F-NaF for each region based on the ratio of ^{18}F-NaF injected dose in ^{18}F$^-$/^{18}F-FDG PET/CT as follows:

$$\text{Adjusted } ^{18}\text{F-NaF uptake value} = \frac{^{18}\text{F}^- \text{ uptake value from } ^{18}\text{F-NaF PET/CT} \times ^{18}\text{F-NaF injected dose in } ^{18}\text{F}^-/^{18}\text{F-FDG PET/CT}}{^{18}\text{F-FDG injected dose in } ^{18}\text{F}^-/^{18}\text{F-FDG PET/CT}}$$

After this, we created estimates of ^{18}F$^-$/^{18}F-FDG uptake value by adding the ^{18}F-FDG uptake value (SUV_{mean} or SUV_{max}) to adjusted ^{18}F-NaF uptake value (SUV_{mean} or SUV_{max}) as follows:

$$\text{Estimated } ^{18}\text{F}^-/^{18}\text{F-FDG uptake value} = ^{18}\text{F-FDG uptake value} + \text{adjusted } ^{18}\text{F-NaF uptake value}$$

Finally, we compared the estimated uptake value with the uptake of actual ^{18}F$^-$/^{18}F-FDG PET/CT.

Statistical Analysis

The data regarding time after injection, injection dose of PET tracers, and SUV are presented as mean ± SD. The Mann–Whitney test was used to compare the difference of injection dose and the scanning start time after PET tracer injection. Pearson correlation coefficient analysis was used for PET uptake and time after injection and among PET uptake including estimated uptake value of ^{18}F$^-$/^{18}F-FDG PET/CT. The Wilcoxon signed-rank test was performed between ^{18}F$^-$/^{18}F-FDG PET/CT, ^{18}F-FDG PET/CT, ^{18}F-NaF PET/CT, and estimated ^{18}F$^-$/^{18}F-FDG PET/CT data to assess the statistical significance of differences between the SUV measurements. All statistical analyses were done with Stata 11 (Stata). Two-tailed P values of less than 0.05 were considered significant.

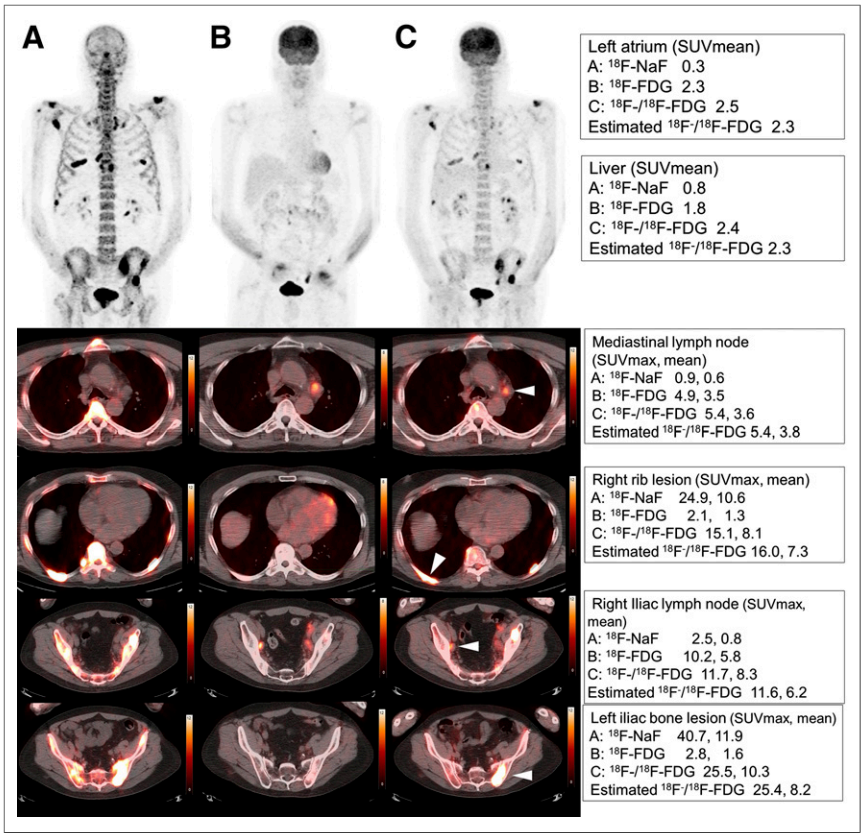

FIGURE 1. A 65-y-old man with metastatic prostate cancer. (A) ^{18}F-NaF. (B) ^{18}F-FDG. (C) ^{18}F$^-$/^{18}F-FDG. SUV_{max} or SUV_{mean} of left atrium, liver, mediastinal lymph node, right rib lesion, left iliac lymph node, and left iliac bone lesion were shown for ^{18}F-NaF, ^{18}F-FDG, and estimated ^{18}F$^-$/^{18}F-FDG, respectively.

RESULTS

^{18}F-FDG and ^{18}F-NaF doses used in ^{18}F$^-$/^{18}F-FDG PET/CT were statistically lower than the doses used in ^{18}F-FDG PET/CT (P = 0.0001) and ^{18}F-NaF PET/CT (P = 0.0003) (Table 1). The time from injection to imaging of ^{18}F$^-$/^{18}F-FDG PET/CT images was not statistically different from those of ^{18}F-FDG (P = 0.54) and ^{18}F-NaF (P = 0.52) (Table 1). The difference in time of starting PET/CT was not significant between ^{18}F$^-$/^{18}F-FDG PET/CT and ^{18}F-FDG PET/CT (P = 0.55) and between ^{18}F$^-$/^{18}F-FDG PET/CT and ^{18}F-NaF PET/CT (P = 0.53).

No significant correlation was noted between uptake and the time from injection to imaging (Table 2). There were no significant difference of SUV_{mean} between ^{18}F$^-$/^{18}F-FDG and ^{18}F-FDG uptake for the cerebral cortex (P = 0.32), cerebellum (P = 0.51), parotid grand (P = 0.77),

TABLE 5
SUV_{mean} and SUV_{max} Measured from PET Scans and Estimated $^{18}F^{-}/^{18}F$-FDG Uptake in Lesions

Value	Lesion	$^{18}F^{-}/^{18}F$-FDG	^{18}F-FDG	^{18}F-NaF	Estimated $^{18}F^{-}/^{18}F$-FDG	*P*		Correlation (r)		
						$^{18}F^{-}/^{18}F$-FDG and ^{18}F-FDG	$^{18}F^{-}/^{18}F$-FDG and estimated $^{18}F^{-}/^{18}F$-FDG	$^{18}F^{-}/^{18}F$-FDG and ^{18}F-FDG	$^{18}F^{-}/^{18}F$-FDG and ^{18}F-NaF	$^{18}F^{-}/^{18}F$-FDG and estimated $^{18}F^{-}/^{18}F$-FDG
SUV_{mean}	All lesions*	7.3 ± 4.6	2.2 ± 1.7	10.0 ± 10.0	6.8 ± 4.2	<0.001	<0.007	0.10	0.84	0.88
	Extraskeletal lesions	4.3 ± 2.4	3.7 ± 2.1	0.9 ± 0.4	4.1 ± 2.1	0.30	0.25	0.90	0.35	0.88
	Skeletal lesions	8.3 ± 4.7	1.7 ± 1.0	12.6 ± 9.9	7.4 ± 4.3	<0.001	<0.001	0.50	0.86	0.92
	Skeletal lesions, PC patient	7.3 ± 4.0	1.5 ± 0.8	10.2 ± 6.7	6.5 ± 3.5	<0.001	<0.003	0.23	0.83	0.85
	Skeletal lesions, non–PC patient	10.5 ± 5.5	2.3 ± 1.2	18.7 ± 13.4	9.6 ± 5.2	<0.001	<0.001	0.69	0.88	0.98
	Osteolytic lesions	10.9 ± 5.5	3.0 ± 1.0	14.5 ± 8.6	9.8 ± 5.1	<0.001	<0.02	0.51	0.88	0.96
	Osteoblastic lesions	7.8 ± 4.4	1.5 ± 0.8	12.3 ± 10.0	7.0 ± 4.0	<0.001	<0.001	0.45	0.86	0.90
	Background†	2.3 ± 0.6	1.8 ± 0.4	1.1 ± 0.4	2.4 ± 0.6	<0.001	0.48	0.70	0.72	0.81
SUV_{max}	All lesions*	15.4 ± 11.4	4.7 ± 4.7	27.4 ± 28.8	16.9 ± 12.4	<0.001	<0.001	0.29	0.82	0.91
	Extraskeletal lesions	9.5 ± 9.4	8.4 ± 6.3	2.2 ± 1.6	9.4 ± 6.7	0.61	0.87	0.94	0.91	0.94
	Skeletal lesions	17.3 ± 11.3	3.4 ± 2.8	34.5 ± 28.9	19.1 ± 12.8	<0.001	<0.002	0.51	0.89	0.91
	Skeletal lesions, PC patient	15.0 ± 9.6	2.7 ± 2.4	29.2 ± 23.9	17.3 ± 12.4	<0.001	<0.001	0.27	0.85	0.88
	Skeletal lesions, non–PC patient	23.0 ± 13.5	5.2 ± 3.0	48.0 ± 35.8	23.8 ± 12.7	<0.001	0.19	0.69	0.91	0.98
	Osteolytic lesions	21.6 ± 9.9	6.8 ± 2.3	36.8 ± 17.7	23.4 ± 8.5	<0.001	0.06	0.34	0.82	0.96
	Osteoblastic lesions	16.6 ± 11.5	2.9 ± 2.5	34.2 ± 30.3	18.4 ± 13.2	<0.001	<0.001	0.52	0.90	0.90
	Background†	3.3 ± 0.8	2.7 ± 0.7	1.8 ± 0.5	3.8 ± 0.9	<0.002	<0.02	0.52	0.52	0.67

*All lesions: both extraskeletal lesions and skeletal lesions.
†Background: uptake at left atrium for patient with malignant lesions.
PC = prostate cancer.

myocardium ($P = 0.94$), and bowel ($P = 0.30$) (Table 3). Therefore, the $^{18}F^{-}/^{18}F$-FDG PET/CT uptake in these organs was estimated to be mainly related to the ^{18}F-FDG uptake. In contrast, the other analyzed organs were estimated to be influenced either by ^{18}F-FDG and ^{18}F-NaF uptake or by only ^{18}F-NaF uptake.

No significant differences were noted between actual $^{18}F^{-}/^{18}F$-FDG uptake and estimated $^{18}F^{-}/^{18}F$-FDG uptake in analyzed organs except the parotid grand related to ^{18}F-FDG ($P < 0.003$) and kidney ($P < 0.02$) (Table 4). Moreover, the correlation between actual $^{18}F^{-}/^{18}F$-FDG uptake and estimated $^{18}F^{-}/^{18}F$-FDG uptake was higher than the correlation between actual $^{18}F^{-}/^{18}F$-FDG uptake and ^{18}F-FDG uptake. The representative image and the SUV of lesions are shown in Figure 1.

The actual $^{18}F^{-}/^{18}F$-FDG uptake in extraskeletal lesions was higher than the ^{18}F-FDG uptake, but this difference has no significance ($P = 0.30$). High correlation was confirmed between $^{18}F^{-}/^{18}F$-FDG uptake and ^{18}F-FDG uptake. Therefore, the influence of ^{18}F-NaF uptake in $^{18}F^{-}/^{18}F$-FDG uptake was estimated to be small (Table 5). In extraskeletal lesions, the T/B ratio from $^{18}F^{-}/^{18}F$-FDG was not significantly different from that of ^{18}F-FDG ($P = 0.73$) (Table 6). The SUV_{mean} in skeletal lesions, regardless of the primary cancer type and the characteristic of the lesion (osteoblastic or osteolytic), was highly influenced by ^{18}F-NaF uptake, estimated from the quite large difference of uptake between $^{18}F^{-}/^{18}F$-FDG and ^{18}F-FDG (Table 5). Regardless of the primary lesion and characteristic of lesion, T/B ratios of $^{18}F^{-}/^{18}F$-FDG for skeletal lesions were statistically lower than the T/B ratio of ^{18}F-NaF ($P < 0.001$) (Table 6). However, this difference did not change the diagnostic ability of $^{18}F^{-}/^{18}F$-FDG PET/CT for the detection of bone lesions, as previously reported (*9*).

DISCUSSION

^{18}F-FDG PET/CT interpretation has relied predominantly on the nuclear medicine physician's experience and knowledge, but using semiquantitative measurement has an advantage to add consistency among interpreters. Our ^{18}F-FDG biodistribution analysis was consistent with previous results (*11–14*), and our ^{18}F-NaF uptake data are similar to those from previous reports analyzing the ^{18}F-NaF uptake in normal bone (*15,16*).

The ^{18}F-NaF PET/CT image showed intense uptake in the skeleton, indicating that $^{18}F^{-}/^{18}F$-FDG uptake in the bony structures was mainly a reflection of ^{18}F-NaF uptake. Compared with bone uptake, the other organs had much lower ^{18}F-NaF uptake, as expected. $^{18}F^{-}/^{18}F$-FDG uptake in the blood pool was significantly higher than ^{18}F-FDG uptake, possibly reflecting additional

TABLE 6
T/B Ratios from PET Scans and Estimated $^{18}F^{-}/^{18}F$-FDG Measurements

Value	Lesion	$^{18}F^{-}/^{18}F$-FDG	^{18}F-FDG	^{18}F-NaF	Estimated $^{18}F^{-}/^{18}F$-FDG	*P*
T/B ratio by SUV_{mean}	All lesions*	3.3 ± 2.2	1.2 ± 1.1	9.3 ± 9.7	2.8 ± 1.7	<0.001
	Extraskeletal lesions	2.1 ± 1.8	2.1 ± 1.8	0.9 ± 0.4	1.9 ± 1.2	0.21
	Skeletal lesions	3.6 ± 2.2	1.0 ± 0.8	11.7 ± 9.7	3.0 ± 1.8	0.006
	Skeletal lesions, prostate cancer patient	3.3 ± 2.0	0.9 ± 0.9	9.4 ± 6.7	2.7 ± 1.5	<0.001
	Skeletal lesions, non–prostate cancer patient	4.4 ± 2.3	1.2 ± 0.6	17.6 ± 13.2	4.0 ± 2.2	<0.005
	Osteolytic lesions	4.6 ± 1.7	1.7 ± 0.6	13.9 ± 6.6	4.3 ± 2.0	0.28
	Osteoblastic lesions	3.4 ± 2.2	0.9 ± 0.8	11.4 ± 10.1	2.8 ± 1.7	<0.001
T/B ratio by SUV_{max}	All lesions*	4.8 ± 3.6	1.7 ± 1.7	14.6 ± 14.0	4.3 ± 3.0	<0.007
	Extraskeletal lesions	3.3 ± 4.2	3.1 ± 2.4	1.4 ± 1.1	2.5 ± 1.9	0.09
	Skeletal lesions	5.2 ± 3.3	1.2 ± 1.2	18.3 ± 13.7	4.8 ± 3.1	<0.03
	Skeletal lesions, prostate cancer patient	4.7 ± 3.1	1.1 ± 1.2	16.0 ± 12.2	4.6 ± 3.1	0.61
	Skeletal lesions, non–prostate cancer patient	6.2 ± 3.6	1.6 ± 1.1	24.2 ± 15.7	5.1 ± 3.1	<0.003
	Osteolytic lesions	6.5 ± 3.0	2.4 ± 1.2	22.9 ± 9.8	6.4 ± 3.3	0.62
	Osteoblastic lesions	5.0 ± 3.3	1.1 ± 1.1	17.6 ± 14.2	4.5 ± 3.0	0.011

*All lesions: both soft-tissue lesions and bone lesions.

^{18}F-NaF present in the blood pool. However, these uptake values are within a small range, which is unlikely to influence the visual interpretation.

Our study also looked at $^{18}F^{-}/^{18}F$-FDG uptake in the lung, pancreas, muscle, and fat, indicating an influence of ^{18}F-NaF uptake on both the ^{18}F-FDG and the ^{18}F-NaF uptake. We estimated $^{18}F^{-}/^{18}F$-FDG uptake as the sum of uptake values and adjusted the ^{18}F-NaF uptake value based on the injection dose of ^{18}F-FDG and ^{18}F-NaF. In all the organs with uptake influenced by both the ^{18}F-FDG and the ^{18}F-NaF uptake, the estimated $^{18}F^{-}/^{18}F$-FDG uptake showed no significant difference with the actual $^{18}F^{-}/^{18}F$-FDG uptake measurements. This indicates that ^{18}F-FDG and ^{18}F-NaF did not have synergistic or offset effect on the $^{18}F^{-}/^{18}F$-FDG PET/CT within the scan time range evaluated in this study.

Osteoblastic lesions generally showed low ^{18}F-FDG uptake; in contrast, osteolytic lesions tend to show high ^{18}F-FDG uptake (*17,18*). ^{18}F-NaF PET/CT has the opposite pattern of uptake (*19*); therefore, ^{18}F-FDG and ^{18}F-NaF PET have drawbacks and advantages for the evaluation of bone lesions and the combination of the 2 provides an advantageous approach for the evaluation of cancer (*20,21*). In addition, in the era of PET/CT, the information from the CT component has additional value in terms of increasing the specificity of the examination (*22*). The combined administration of $^{18}F^{-}/^{18}F$-FDG in a single PET/CT can detect both extraskeletal and skeletal lesions in a single scan, indicating the potential for 1-stop-shop examination for cancer staging (*9,10*).

A limitation of this study was the selection bias toward patients with known cancers. Although there were no significant difference of SUV in most organs in this study, variations in injected dosage, time from injection to imaging, and lack of direct measurements such as arterial sampling and dynamic imaging were additional limitations in this assessment. Scans conducted at different times after injection might result in significantly different average SUVs of malignant lesion. The optimal ratios of ^{18}F-NaF to ^{18}F-FDG in $^{18}F^{-}/^{18}F$-FDG PET/CT scan have been an issue for this combined method. According to a preclinical study, the optimal ratio of ^{18}F-NaF to ^{18}F-FDG was 1–5 for the contrast resolution (*23*). Although further clinical studies are required to confirm these assessments, our results and methodology in this study may contribute to this work.

CONCLUSION

The understanding of the biodistribution of radiopharmaceuticals and the lesion uptake of the $^{18}F^{-}/^{18}F$-FDG scan, as well as the variations, compared with the uptake on the separate ^{18}F-FDG PET/CT and ^{18}F-NaF PET/CT are valuable for more in-depth evaluation of the combined scanning technique.

DISCLOSURE

The costs of publication of this article were defrayed in part by the payment of page charges. Therefore, and solely to indicate this fact, this article is hereby marked "advertisement" in accordance with 18 USC section 1734. No potential conflict of interest relevant to this article was reported.

ACKNOWLEDGMENTS

We thank our research coordinator Euodia Jonathan; Jarrett Rosenberg, PhD, for statistical support; Frederick Chin, PhD; the staff at the Lucas Cyclotron; and the technologists in the Division

of Nuclear Medicine and Molecular Imaging. We extend special thanks to all our patients and their families.

REFERENCES

1. Gambhir SS. Molecular imaging of cancer with positron emission tomography. *Nat Rev Cancer.* 2002;2:683–693.
2. Cook GJ, Fogelman I. The role of positron emission tomography in skeletal disease. *Semin Nucl Med.* 2001;31:50–61.
3. Hoh CK, Hawkins RA, Dahlbom M, et al. Whole body skeletal imaging with [^{18}F]fluoride ion and PET. *J Comput Assist Tomogr.* 1993;17:34–41.
4. Grant FD, Fahey FH, Packard AB, et al. Skeletal PET with ^{18}F-fluoride: applying new technology to an old tracer. *J Nucl Med.* 2008;49:68–78.
5. Even-Sapir E, Metser U, Flusser G, et al. Assessment of malignant skeletal disease: initial experience with ^{18}F-fluoride PET/CT and comparison between ^{18}F-fluoride PET and ^{18}F-fluoride PET/CT. *J Nucl Med.* 2004;45:272–278.
6. Mosci C, Iagaru A. ^{18}F NaF PET/CT in the assessment of malignant bone disease. *PET Clin.* 2012;7:263–274.
7. Tateishi U, Morita S, Taguri M, et al. A meta-analysis of ^{18}F-fluoride positron emission tomography for assessment of metastatic bone tumor. *Ann Nucl Med.* 2010;24:523–531.
8. Lin FI, Rao J, Mittra E, et al. Prospective comparison of combined ^{18}F-FDG and ^{18}F-NaF PET/CT vs. ^{18}F-FDG PET/CT imaging for detection of malignancy. *Eur J Nucl Med Mol Imaging.* 2012;39:262–270.
9. Iagaru A, Mittra E, Yaghoubi SS, et al. Novel strategy for a cocktail ^{18}F-fluoride and ^{18}F-FDG PET/CT scan for evaluation of malignancy: results of the pilot-phase study. *J Nucl Med.* 2009;50:501–505.
10. Iagaru A, Mittra E, Mosci C, et al. Combined ^{18}F-fluoride and ^{18}F-FDG PET/CT scanning for evaluation of malignancy: results of an international multicenter trial. *J Nucl Med.* 2013;54:176–183.
11. Wang Y, Chiu E, Rosenberg J, Gambhir SS. Standardized uptake value atlas: characterization of physiological 2-deoxy-2-[^{18}F]fluoro-D-glucose uptake in normal tissues. *Mol Imaging Biol.* 2007;9:83–90.
12. Tan LT, Ong KL. Semi-quantitative measurements of normal organs with variable metabolic activity on FDG PET imaging. *Ann Acad Med Singapore.* 2004;33:183–185.
13. Zincirkeser S, Sahin E, Halac M, Sager S. Standardized uptake values of normal organs on ^{18}F-fluorodeoxyglucose positron emission tomography and computed tomography imaging. *J Int Med Res.* 2007;35:231–236.
14. Chin BB, Green ED, Turkington TG, Hawk TC, Coleman RE. Increasing uptake time in FDG-PET: standardized uptake values in normal tissues at 1 versus 3 h. *Mol Imaging Biol.* 2009;11:118–122.
15. Frost ML, Blake GM, Park-Holohan SJ, et al. Long-term precision of ^{18}F-fluoride PET skeletal kinetic studies in the assessment of bone metabolism. *J Nucl Med.* 2008;49:700–707.
16. Sachpekidis C, Goldschmidt H, Hose D, et al. PET/CT studies of multiple myeloma using ^{18}F-FDG and ^{18}F-NaF: comparison of distribution patterns and tracers' pharmacokinetics. *Eur J Nucl Med Mol Imaging.* 2014;41:1343–1353.
17. Hsu WK, Virk MS, Feeley BT, Stout DB, Chatziioannou AF, Lieberman JR. Characterization of osteolytic, osteoblastic, and mixed lesions in a prostate cancer mouse model using ^{18}F-FDG and ^{18}F-fluoride PET/CT. *J Nucl Med.* 2008;49:414–421.
18. Nakai T, Okuyama C, Kubota T, et al. Pitfalls of FDG-PET for the diagnosis of osteoblastic bone metastases in patients with breast cancer. *Eur J Nucl Med Mol Imaging.* 2005;32:1253–1258.
19. Cook GJ, Fogelman I. The role of positron emission tomography in the management of bone metastases. *Cancer.* 2000;88:2927–2933.
20. Hoegerle S, Juengling F, Otte A, Altehoefer C, Moser EA, Nitzsche EU. Combined FDG and [F-18]fluoride whole-body PET: a feasible two-in-one approach to cancer imaging? *Radiology.* 1998;209:253–258.
21. Cook GJ, Fogelman I. Detection of bone metastases in cancer patients by ^{18}F-fluoride and ^{18}F-fluorodeoxyglucose positron emission tomography. *Q J Nucl Med.* 2001;45:47–52.
22. Sampath SC, Sampath S, Mosci C, et al. Detection of osseous metastasis by ^{18}F-NaF/^{18}F-FDG PET/CT versus CT alone. *Clin Nucl Med.* 2015;40:e173–e177.
23. Richmond K, McLean N, Rold T, Szczodroski A, Dresser T, Hoffman T. Optimizing a F-18 NaF and FDG cocktail as a preclinical cancer screening tool for molecular imaging [abstract]. *J Nucl Med.* 2011;52(suppl 1):2455.